Exciton localization in tubular molecular aggregates

Bondarenko, Anna S.; Jansen, Thomas L. C.; Knoester, Jasper

Link to publication in University of Groningen/UMCG research database

Exciton localization in tubular molecular aggregates: Size effects and optical response

Anna S. Bondarenko (iD), Thomas L. C. Jansen (iD), and Jasper Knoester (iD)

View Online   **Export Citation**   **CrossMark**

Exciton localization in tubular molecular aggregates: Size effects and optical response

View Online   Export Citation   CrossMark

Anna S. Bondarenko, (iD) Thomas L. C. Jansen, (iD) and Jasper Knoester[a] (iD)

AFFILIATIONS

Zernike Institute for Advanced Materials, University of Groningen, Nijenborgh 4, 9747 AG Groningen, The Netherlands

[a]Author to whom correspondence should be addressed: j.knoester@rug.nl

ABSTRACT

We study the exciton localization and resulting optical response for disordered tubular aggregates of optically active molecules. It has previously been shown that such tubular structures allow for excitons delocalized over more than a thousand molecules, owing to the combined effects of long-range dipole–dipole interactions and the higher-dimensional (not truly one-dimensional) nature of the aggregate. Such large delocalization sizes prompt the question to what extent in experimental systems the delocalization may still be determined by the aggregate size (diameter and length) and how this affects the aggregate's optical response and dynamics. We perform a systematic study of the size effects on the localization properties using numerical simulations of the exciton states in a cylindrical model structure inspired by the previously derived geometry of a cylindrical aggregate of cyanine dye molecules (C8S3). To characterize the exciton localization, we calculate the participation ratio and the autocorrelation function of the exciton wave function. We also calculate the density of states and absorption spectrum. We find strong effects of the tube's radius on the localization and optical properties in the range of parameters relevant to the experiment. In addition, surprisingly, we find that even for tubes as long as 750 nm, the localization size is limited by the tube's length for disorder values that are relevant to experimental circumstances, while observable effects of the tube's length in the absorption spectrum still occur for tube lengths up to about 150 nm. The latter may explain the changes in the optical spectra observed during the aging process of bromine-substituted C8S3 aggregates. For weak disorder, the exciton wave functions exhibit a scattered, fractal-like nature, similar to the quasi-particles in two-dimensional disordered systems.

I. INTRODUCTION

Self-assembled aggregates of molecules with strong optical transitions have been studied abundantly for more than 80 years now.[1–3] The close packing of molecules within such aggregates gives rise to collective optically allowed excited states, Frenkel excitons, that are shared by a number of molecules and that give rise to interesting optical phenomena. Examples are exchange narrowing of spectral lineshapes,[4,5] collective spontaneous emission,[6,7] a Pauli-exclusion gap measured in pump–probe spectroscopy,[8,9] and enhanced nonlinear optical properties.[10,11] Typically, such aggregates also exhibit fast excitation energy transport, reflected, for instance, in very high exciton–exciton annihilation efficiencies.[12] Synthetic dye aggregates consisting of many thousands of molecules, in particular those prepared from cyanine dye molecules, have played a crucial role in the development of color photography and xerography.[13–15] On the other hand, natural aggregates consisting of optically active biomolecules have also received much attention lately, in particular, in the context of light-harvesting antenna complexes in the photosynthetic systems of bacteria, algae, and higher plants.[16–19] Such aggregates, mainly consisting of (bacterio)chlorophyll molecules, usually stabilized in a protein scaffold, have the purpose of absorbing the energy of the sunlight, thereby converting it into an electronic excitation, which subsequently is transported with high efficiency (quantum efficiencies over 90%) to the photosynthetic reaction center to trigger the first step in the photochemical reaction. The extent to which delocalized and quantum coherent excitons play a role in natural antenna systems has been a topic of much interest during the past 20 years.[19–31]

The role of collective effects in the optical response and excited state dynamics of molecular aggregates depends on how many molecules share an excitation, a quantity known as the exciton delocalization size. In ideal, nicely ordered aggregates of identical molecules, in principle, the excitations are shared by all molecules.

In practice, however, disorder in the transition energies of individual molecules imposed by an inhomogeneous host medium and disorder in the excitation transfer interactions between molecules, resulting from structural fluctuations, limit the exciton delocalization to much smaller numbers. In the prototypical aggregates of the synthetic dye molecule pseudo-isocyanine (PIC), the delocalization size at low temperatures is in the order of 50–70 molecules,[8,32] which is large enough to see strong collective effects, but still considerably smaller than the many thousands of molecules that make up these aggregates. The strong localization effect results from the one-dimensional character of PIC aggregates.

During the past 15 years, a large number of tubular molecular aggregates have been studied, synthetic,[33–52] semi-synthetic,[45,53] and natural[54–57] ones. These systems typically have diameters in the order of 10 nm and lengths of 100 nm up to micrometers. This renders them quasi-one-dimensional systems from a geometrical point of view that might, for instance, serve as excitation energy transport wires. However, it has been shown that the extra dimension (the tube's circumference) in combination with the long-range (dipolar) intermolecular excitation transfer interactions leads to much weaker exciton localization than in truly one-dimensional systems.[58] This explains experiments on a variety of tubular aggregates, demonstrating strong dependence of the optical properties on the polarization direction of the absorbed or emitted light relative to the tube's axis.[33,34,38,40,57] In fact, the delocalization size in tubular aggregates of the dye C8S3 was estimated to be in the order of a thousand molecules, even in the optically dominant energy region near the exciton band edge, where localization properties are strongest.[58]

The large exciton delocalization sizes in tubular aggregates are of direct relevance to their optical and excitation transport properties. For instance, it has been shown that the exciton diffusion constant in tubular model aggregates is a universal function of the ratio of the exciton localization length and the cylinder's circumference.[59] This becomes all the more interesting because recently, some degree of control of the radius of a tubular aggregate of cyanine molecules has been reported.[60] Moreover, given the large delocalization sizes obtained in numerical simulations, the question arises to what extent the system size still plays a role in their value, both in the calculation and in the experiment. Thus far, a systematic study of size effects in the localization properties, and hence the optical properties, has not been performed.

In this work, we numerically investigate the dependence of the exciton localization properties and absorption spectrum on both the radius and the length of tubular molecular aggregates. We employ a Frenkel exciton model with Gaussian site disorder on an experimentally relevant tubular aggregate structure. The findings confirm that under experimental conditions, it is possible that the delocalization is not solely determined by the ratio of the strength of the disorder and the width of the exciton band but also by the aggregate size. We also show that this does not imply that the excitons are spread over the entire system in the same way as the excitons in a homogeneous tubular aggregate are spread; rather the wave functions seem to be spread in a highly irregular way, resembling fractal behavior.[61]

The outline of this paper is as follows: In Sec. II, we describe the details of the model used in our study and the approach; in particular, we define the various quantities studied in our analysis. Next, in Sec. III, we present our results, followed by a discussion. Finally, in Sec. IV, we conclude. In the Appendix, several details are presented that characterize the exciton band as a function of system size.

II. MODEL AND APPROACH

A. Structural model

Throughout this paper, we use as the model system the extended herringbone model introduced in Ref. 39 to describe the inner wall of the frequently studied double-walled tubular molecular aggregates of the dye C8S3 [3,3′-bis(2-sulfopropyl)-5,5′,6,6′-tetrachloro-1,1′-dioctylbenzimidacarbocyanine]. We stress that the purpose of this study is not to give detailed fits for C8S3 aggregates, but to study generic effects that may occur under experimentally relevant conditions in disordered tubular aggregates as a function of length and radius. The model considered describes a single-walled tubular aggregate with two identical molecules per unit cell, which only differ from each other by their position in the unit cell and their orientation in the local frame of the tube. For the purpose of describing the optical properties, all molecules are considered two-level systems with an optical transition dipole between the ground state and the excited state, which is fixed to the molecular frame. The model may be considered as a perpendicular stack of N_1 equidistant rings, separated by a distance h, where on each ring, the positions of N_2 equidistant unit cells are located. Neighboring rings are rotated relative to each other over a helical angle γ.

The above described packing is realized by wrapping a planar two-dimensional lattice with two molecules per unit cell (which are tilted out of the plane) on a cylindrical surface. This wrapping is fully dictated by the length and direction of the vector over which the lattice is rolled; the length of the rolling vector gives the circumference of the cylinder (and hence dictates the radius of the tube). The parameter h only depends on the orientation of the rolling vector and the lattice constants, while both N_2 and γ also depend on its length. Throughout this work, the orientation of the rolling vector was kept fixed and equal to the one used for the inner wall in Ref. 39 to fit the experimental spectrum of C8S3 tubes, leading to a fixed value of $h = 0.2956$ nm. In order to allow us to investigate the dependence of the tube's localization and optical properties on its radius, the length of the rolling vector was varied. This means that only a discrete set of radii can be considered because after wrapping the two-dimensional lattice on the cylinder, the molecule where the rolling vector starts should coincide with the one where it ends (seamless wrapping). For further details of creating the structural model, in particular, the lattice parameters, the tilt angles, and the orientation of the rolling vector, we refer to Refs. 39 and 60.

The variation in radii considered in our calculations is such that N_2 takes all integer values in the range $N_2 = 1, \ldots, 35$. Within the model considered here, the inner tube of the C8S3 aggregates has $N_2 = 6$, while the inner wall of the wider bromine-substituted C8S3 [3,3′-bis(2-sulfopropyl)-5,5′,6,6′-tetrabromo-1,1′-dioctylbenzimidacarbocyanine] aggregates has a radius, which due to a slightly different lattice approximately corresponds to $N_2 = 11$, both values that fall inside the range of radii studied here. When investigating the radius dependence, the length was kept fixed at $N_1 = 666$, which agrees with a physical length of 196.9 nm. When

studying the length dependence, the radius was kept fixed at 3.5505 nm, which agrees with a ring of $N_2 = 6$ unit cells, the value that applies to the inner wall of unsubstituted C8S3. We then considered 11 different values for the length lying between $N_1 = 170$ and $N_1 = 2500$, i.e., a physical length between 50 nm and 740 nm, which is an experimentally relevant range. The total number of molecules in the aggregate thus ranges from 1332 to 46 620 for the smallest and largest radii, respectively.

B. Model Hamiltonian

The collective optical (charge neutral) excited states of the aggregate are described by the Frenkel exciton Hamiltonian,

$$H = \sum_{n,m} H_{nm} |n\rangle\langle m| = \sum_n (\omega_0 + \Delta_n)|n\rangle\langle n| + \sum_{n\neq m} J_{nm}|n\rangle\langle m|, \quad (1)$$

where n and m run over all molecules and $|n\rangle$ denotes the state where molecule n is excited and all other molecules are in their ground state. Throughout this paper, we use open boundary conditions at the top and bottom rings of the cylinder (i.e., the cylinder is not folded into a torus).

The first term in Eq. (1) describes the molecular excited state energy ($\hbar = 1$), where ω_0 gives the mean value, which is taken to be 18 868 cm^{-1},[39] and the offset Δ_n describes the energy disorder that gives rise to localization. We will model the disorder by randomly choosing the Δ_n from a Gaussian distribution with mean zero and standard deviation σ; the disorder offsets on different molecules are assumed to be uncorrelated from each other. The second term in Eq. (1) describes the intermolecular excitation transfer interactions, which are described by extended dipole–dipole interactions between all molecules, using $q = 0.34e$ and $l = 0.7$ nm, respectively, for the point charges and length of the vector connecting them.[39] No disorder in the interactions J_{nm} is considered in this paper, i.e., we do not take into account the structural disorder. The interactions J_{nm} promote the delocalization of the excitation over the aggregate. For the structure considered here, the interactions are strong, owing to the fact that the C8S3 molecules have a large transition dipole (11.4 Debye)[39] and have small separations between each other. Based on this, the strongest four interactions have an absolute value between 1000 cm^{-1} and 1500 cm^{-1}, while the next three largest interactions all are in the order of -500 cm^{-1}.

In order to study the localization and optical properties of the aggregate, we first numerically diagonalize the Hamiltonian for a particular disorder realization, which provides us with the eigenstate $|q\rangle = \sum_n \varphi_{qn}|n\rangle$ and its energy ω_q, where φ_{qn} and ω_q denote the eigenvectors (normalized to unity) and eigenvalues, respectively, of the matrix H_{nm}. From these quantities, all properties that we are interested in follow. Specifically, the exciton density of states (DOS) is given by

$$\rho(\omega) = \left\langle \sum_q \delta(\omega - \omega_q) \right\rangle, \quad (2)$$

where the angular brackets denote an average over disorder realizations. Similarly, the absorption spectrum is given by

$$A(\omega) = \left\langle \sum_q |\vec{e} \cdot \vec{\mu}_q|^2 \delta(\omega - \omega_q) \right\rangle, \quad (3)$$

where $\vec{e}$ denotes the electric polarization vector of the light used to take the spectrum and $\vec{\mu}_q = \sum_n \varphi_{qn}\vec{\mu}_n$ is the transition dipole between the aggregate's ground state (all molecules in their ground state) and the exciton state $|q\rangle$, with $\vec{\mu}_n$ denoting the transition dipole vector of molecule n.

C. Wavefunction characterization

To characterize the exciton localization properties, we study two quantities. The first one is the inverse participation ratio, defined as[62,63]

$$\mathcal{P}^{-1}(\omega) = \frac{\left\langle \sum_q \delta(\omega - \omega_q) \sum_n |\varphi_{qn}|^4 \right\rangle}{\rho(\omega)}. \quad (4)$$

The inverse participation ratio equals 1 for states localized on one molecule only, while for states that are equally shared by all molecules of the aggregate, its value equals $1/N$, where N is the total number of molecules. Alternatively, the reciprocal of the inverse participation ratio, also known as the participation ratio, $\mathcal{P}(\omega)$, is generally accepted as a quantity that characterizes how many molecules take part in (share) the collective excitations at energy ω. Depending on the disorder strength and the exciton energy, this value may be anywhere between unity (totally localized state) and αN (totally delocalized state), where α is a constant in the order of unity, which depends on whether open or closed boundary conditions are used. In general, the localization properties depend on energy ω, as is made explicit in the above notation.

The second quantity that we will use to investigate the extended nature of the exciton states is the autocorrelation function of the exciton wave function,[64] derived from

$$C_{ij}(\mathbf{s};\omega) = \frac{N_1}{N_1 - |s_1|} \frac{\left\langle \sum_q \sum_{\mathbf{n}} |\varphi_q(\mathbf{n},i)\varphi_q^\star(\mathbf{n}+\mathbf{s},j)|\delta(\omega - \omega_q) \right\rangle}{\rho(\omega)}, \quad (5)$$

where a two-dimensional vector notation has been introduced to indicate the position of the unit cell and i and j can both take on the values 1 and 2 in order to label the different molecules within the unit cell. Thus, $\mathbf{n} = (n_1, n_2)$, with $n_1 = 1, \ldots, N_1$ labeling the ring on which the unit cell resides and $n_2 = 1, \ldots, N_2$ indicating its position in the ring. Because the aggregate has open boundary conditions in the n_1 direction, the number of terms in the summation over n_1 is limited by the value of s_1. This would possibly result in an artificial fast drop of the correlation function with growing $|s_1|$; in order to account for this, the correction factor $N_1/(N_1 - |s_1|)$ has been added. A similar correction is not needed for the n_2 summation as in the ring direction, periodic boundary conditions are inherently included in the system, always allowing for N_2 terms in the summation over n_2.

C_{ij} defined above is a 2×2 matrix, whose elements show an overall similar decay behavior for localized states. In order to just present one quantity, we have chosen to focus on one specific correlation function defined through the trace of the matrix,

$$C(\mathbf{s};\omega) = C_{11}(\mathbf{s};\omega) + C_{22}(\mathbf{s};\omega), \quad (6)$$

which has the nice property that its value at the origin is normalized to unity at all energies: $C(\mathbf{s} = \mathbf{0}; \omega) = 1$. From the autocorrelation function, we may extract another localization measure $N_{\mathrm{corr}}(\omega)$ as a function of energy as the number of molecules for which $|C(\mathbf{s}; \omega)| > 1/e$.[64] We will also be particularly interested in the autocorrelation function along the tube's axis and define the correlation length $N_{\|,\mathrm{corr}}(\omega)$ as the number of rings for which $|C(s_1, s_2 = 0, \omega)| > 1/e$. $N_{\|,\mathrm{corr}}$ is a measure of the number of rings over which the exciton wave functions are delocalized.

In the results presented in Sec. III, the number of disorder realizations used to evaluate the disorder average $\langle \cdots \rangle$ was taken to be 150.

III. RESULTS AND DISCUSSION

A. Absorption spectra

We start from studying how the optical properties depend on the tube's size (length and radius) and on the disorder. A typical absorption spectrum of the tubular aggregate studied here is shown in Fig. 1(a) for a structure with length $N_1 = 666$ and radius $N_2 = 6$. The stick spectrum of the homogeneous structure features four J bands: two bands polarized parallel to the tube's axes (red lines) and two bands polarized perpendicular to it (blue lines). These bands originate from the selection rules dictated by the cylindrical symmetry of the structure.[65] The eigenstates of the homogeneous tubular aggregate have Bloch character in the ring direction characterized by a transverse quantum number k_2.[65] The optically allowed states occur in the bands of states with $k_2 = 0$ (polarized parallel to the tube's axis) and those with $k_2 = \pm 1$ (degenerate and polarized perpendicular to the axis). Moreover, the lattice with two molecules per unit cell used in this study gives rise to a Davydov splitting, resulting in the four optical bands observed in Fig. 1(a). Our main interest is the low-energy Davydov component of the $k_2 = 0$ band as this optical band lies close to the bottom of the exciton band [see Fig. 1(b)]

and, therefore, has a linewidth that is primarily determined by static disorder.

Disorder gives rise to broadening and an energy shift of the optical bands compared to the homogeneous stick spectrum. This is shown in Fig. 1(a), where light red and light blue lines show the spectrum in both polarization directions for tubes with (weak) disorder strength given by $\sigma = 180$ cm^{-1}. The disorder strength of 180 cm^{-1} is used as in the model considered here; this explains the broadening of the lowest-energy J band for bromine-substituted C8S3 aggregates observed in the experiment.[60] The broadening and energy shift are a result of the breaking of the selection rules by the disorder and the resulting mixing of states with different k_2 values. The density of states for this system is shown in Fig. 1(b) together with the absorption spectrum. The exciton band exhibits a marked asymmetry around its center as a result of the inclusion of long-range interactions.[32] The lowest-energy optical band lies slightly above the lower exciton band edge. The energy dependence of the density of states reflects sharp peaks due to the one-dimensional sub-bands for different k_2 values, which persist for the weak disorder value of $\sigma = 180$ cm^{-1}.

1. Length dependence

We first examine the effect of the tube's length on the absorption spectrum. Figure 2 displays the calculated position of the lowest-energy optical band as a function of the tube's length in the presence of disorder. This figure suggests that observable changes in the position of this band occur for tubes with lengths up to 150 nm ($N_1 = 510$). Specifically, a red shift of 50 cm^{-1} arises between the tubes with $N_1 = 170$ and $N_1 = 510$, corresponding to an increase in the length from 50 nm to 150 nm. For $N_1 > 510$, the calculated energy position of the optical bands essentially does not change. Our theoretical calculations are in qualitative agreement with the experimentally observed red shift of the parallel polarized band during the aging process of bromine-substituted C8S3 aggregate solutions:
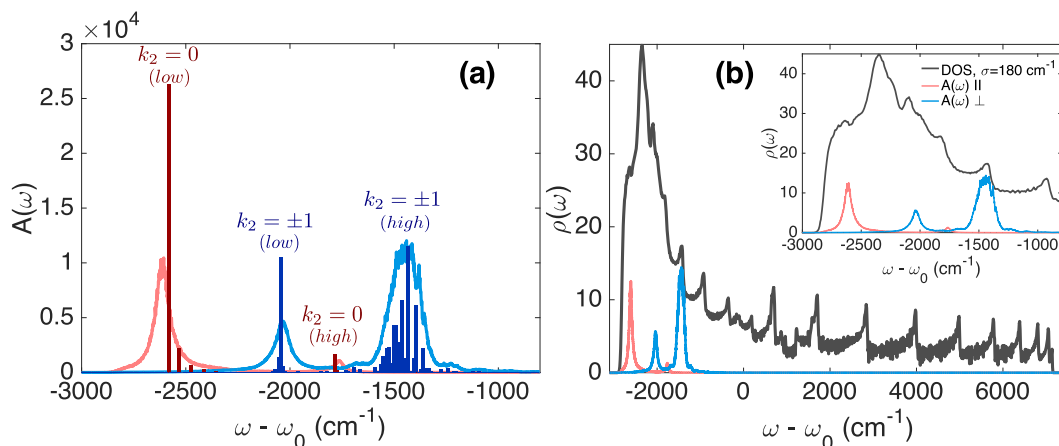
FIG. 1. (a) Typical absorption spectrum: homogeneous limit vs disordered case. The stick spectrum of a homogeneous tubular aggregate with $N_1 = 666$ and $N_2 = 6$ is shown together with the spectrum in the presence of disorder with $\sigma = 180$ cm^{-1}. The absorption spectrum has four optical band regions: those polarized parallel (red) and perpendicular (blue) to the tube's axis, each having low- and high-energy Davydov components. In the absence of disorder, the low-energy $k_2 = 0$ Davydov peak lies 172 cm^{-1} above the exciton band edge. (b) DOS of the same system with $\sigma = 180$ cm^{-1}, plotted together with the absorption spectrum depicted in (a). The inset shows a magnification of the region of the absorption bands.

FIG. 2. Dependence of the position of the simulated lowest-energy optical band on the tube's length for tubes with $N_2 = 6$ and N_1 ranging from 170 to 1666 for $\sigma = 180$ cm^{-1}.

using cryo-TEM imaging, the tube's length was seen to grow while aging.[66]

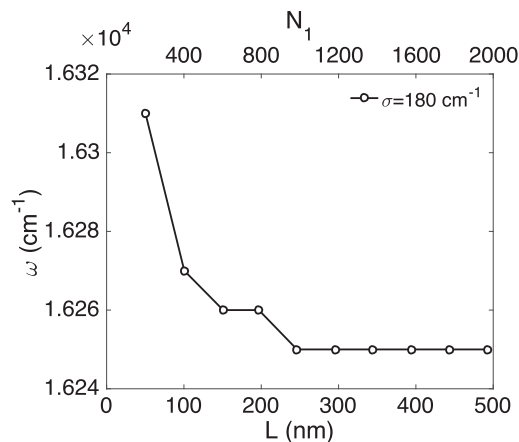Next, we examine the overall line shape of the absorption spectra of large tubes in the presence of disorder. Figures 3(a) and 3(b) present the absorption spectra of two tubes with the same radius ($N_2 = 6$) but different lengths, decomposed in parallel (red) and perpendicular (blue) bands. The two tubes have a length of $N_1 = 833$ (L1) and $N_1 = 1666$ (L2) and are shown in darker and lighter colors, respectively. Absorption spectra of the tubes with weak [$\sigma = 180$ cm^{-1}, Fig. 3(a)] and strong [$\sigma = 800$ cm^{-1}, Fig. 3(b)] disorder are shown together with the stick spectra in the absence of disorder. As can be seen, both for weak and strong disorder, the width and energy position of parallel and perpendicular bands do not change anymore with an increase in length in this N_1 region. This is somewhat surprising in the light of the fact observed later on Sec. III B that at least for $\sigma = 180$ cm^{-1}, the exciton delocalization size still grows with the tube's length in this region. This implies that exchange narrowing of the absorption bands—the effect that the absorption band width is inversely proportional to the square root
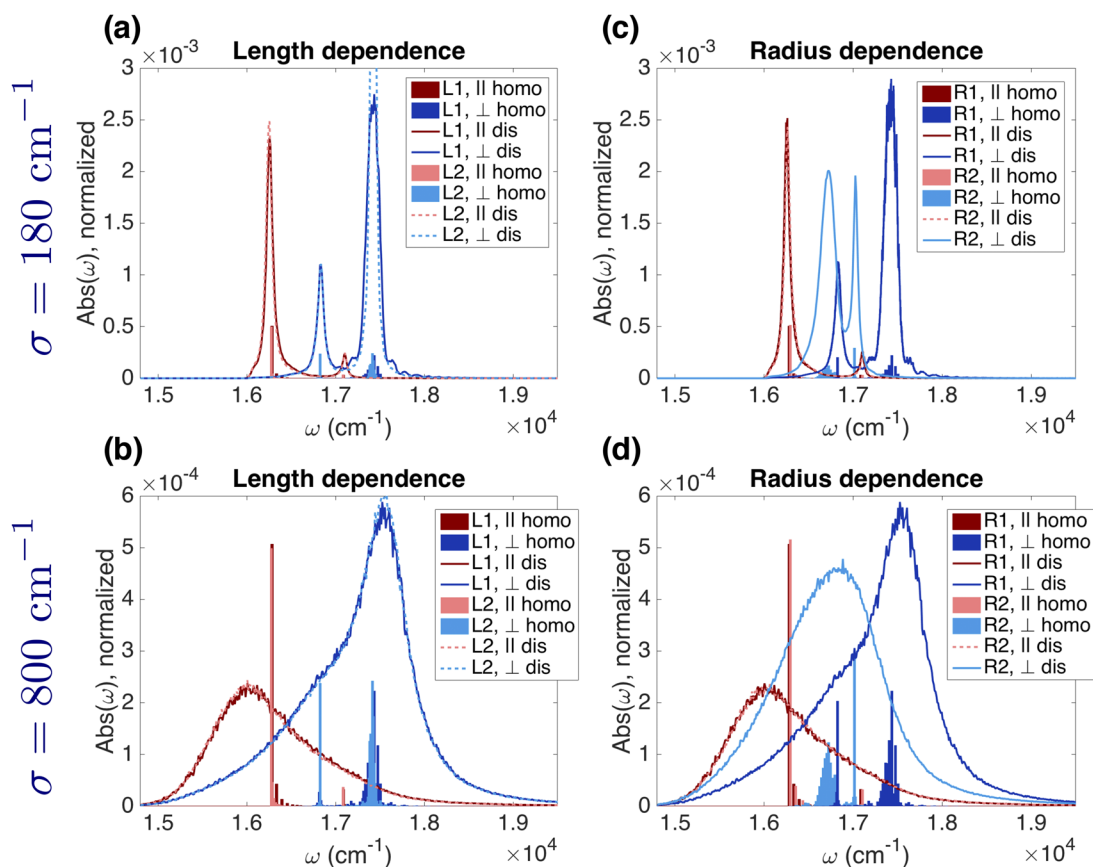

FIG. 3. Length and radius dependence of the absorption spectra. Parallel (red colors) and perpendicular (blue colors) polarized bands of the absorption spectra are presented for two different lengths [(a) and (b)] and two different radii [(c) and (d)] for weak [(a) and (c)] and stronger [(b) and (d)] disorder. The length dependence of the absorption spectra is shown for tubes of fixed radius ($N_2 = 6$) and smaller length L1, $N_1 = 833$ (dark red and dark blue), and larger length L2, $N_1 = 1666$ (light red and light blue). The radius dependence of the absorption spectra is presented for tubes with fixed length ($N_1 = 666$) and smaller radius R1, $N_2 = 6$, (dark red and dark blue) and larger radius R2, $N_2 = 15$, (light red and light blue). The spectra of the disordered systems for both length and radius dependencies are shown together with the homogeneous stick spectra with the same color scheme. The disordered absorption spectra were normalized to the area under the spectrum. The homogeneous stick spectra were scaled by a factor of 0.02 to facilitate the comparison.

of the delocalization size, common for one-dimensional aggregates with uncorrelated Gaussian disorder[4,32]—does not occur here. This may be related to the special character of the exciton states discussed later on Sec. III D and the very high density of states in the optically relevant region of the spectrum, where bands with different k_2 values are easily mixed by disorder.

2. Radius dependence

Next, we study the effect of the tube's radius on the absorption spectrum. Figures 3(c) and 3(d) present the parallel (red) and perpendicular (blue) polarized contributions of the absorption spectra of tubes of the same length (N_1 = 666) and different radii; darker and lighter colors correspond to tubes with N_2 = 6 (R1) and N_2 = 15 (R2), respectively. Increasing the tube's radius gives rise to considerable changes in the absorption spectra, which primarily originates from the radius dependence of the energy position of the perpendicular polarized optical bands.[65] The width and position of the lowest-energy optical band are hardly sensitive to the radius. This is true for both values of the disorder, σ = 180 cm^{-1} [Fig. 3(c)] and σ = 800 cm^{-1} [Fig. 3(d)]. The dependence of the energy position of the perpendicular polarized band on the tube's radius is the main cause of the changes in the absorption spectrum experimentally observed when replacing four chlorine atoms by bromine atoms in C8S3 molecules, which leads to larger radii of the self-assembled nanotubes.[60]

3. Disorder scaling of absorption band width and position

Next, we examine the disorder dependence of the optical band width, W, and red shift, S, of the lowest-energy J band. To this end, we first fit the absorption spectrum to a sum of Gaussian line shapes in order to isolate this J band. Then, we take the full width at half maximum of the corresponding Gaussian as W. For S, we use the difference between the mean value of the corresponding Gaussian and the energy position of the lowest-energy peak in the stick spectrum. The obtained results for W and S are presented in Figs. 4(a) and 4(b), respectively, as a function of the disorder strength. Both

dependencies may be fitted well by a power law (curves in Fig. 4), as is common for a variety of molecular aggregates.[32,58,67–70] For the width, the best fit according to $W = a\sigma^b$ yields b = 1.51 [Fig. 4(a)]. The obtained exponent is higher than the value of 1.34 obtained for one-dimensional J aggregates.[32,67–69] However, it is considerably smaller than the value of 2.83 obtained from a previous study on tubular aggregates.[58] The strong difference with Ref. 58 can be explained from the differences in the exciton density of states at the position of the lowest-energy J band, which, in turn, can be traced back to differences in the lattice structure. In the case of Ref. 58, a tube with one molecule per unit cell was considered with a lattice structure, which near the lower band-edge gives rise to a low density of states, scaling with the square-root of energy; in our case, the density of states is rather high already at the position of the lowest-energy band and does not seem to depend strongly on energy [Fig. 1(b)]. The result is a scaling of W with disorder that is much closer to the one-dimensional case.

The results for the scaling of the energy shift with disorder [Fig. 4(b)] show similar behavior as the absorption band width. The value of 1.52 for the exponent in the corresponding power law fit is somewhat larger than the value of 1.35 found for the one-dimensional system.[32] The increase in the red shift reaches a maximum at σ = 1200 cm^{-1} and then starts to decrease again. This may be explained from the fact that for disorder values larger than the exciton bandwidth, the interactions are relatively unimportant, and the spectrum should tend to a very broad peak, centered at the monomer transition frequency.

B. Degree of localization: Participation number

In this section, we establish the behavior of the degree of localization of the eigenstates obtained from the participation number calculated using Eq. (4). The energy dependence of this quantity multiplied by 9/4 is shown in Fig. 5 for σ = 180 cm^{-1} and σ = 800 cm^{-1}, where the factor 9/4 was introduced to ensure that in the homogeneous limit (σ = 0 cm^{-1}), this number tends to the system size $2N_1N_2$[64] (the factor of 2 stems from the fact that we deal with tubes with two molecules per unit cell). Clearly, with the
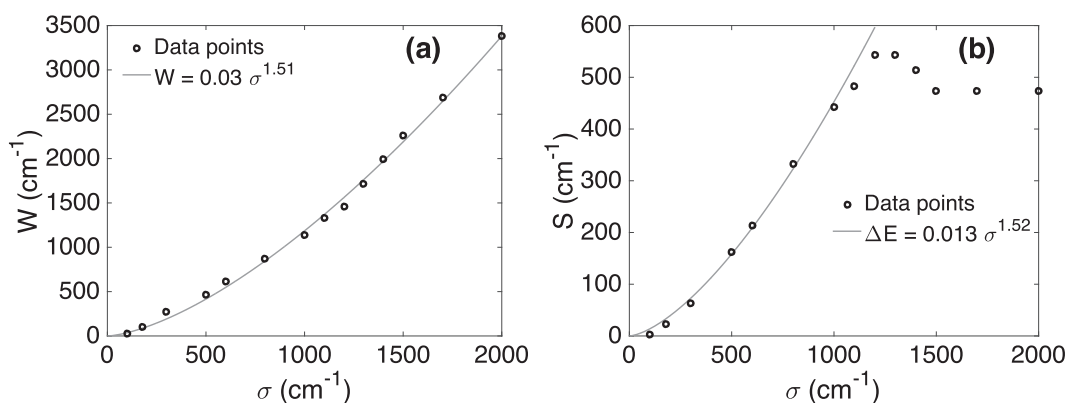

FIG. 4. Disorder scaling of the absorption properties of the tube aggregate: (a) FWHM, or W, and (b) red shift, or S, of the lowest-energy absorption band of tubes with N_1 = 666 and N_2 = 6.
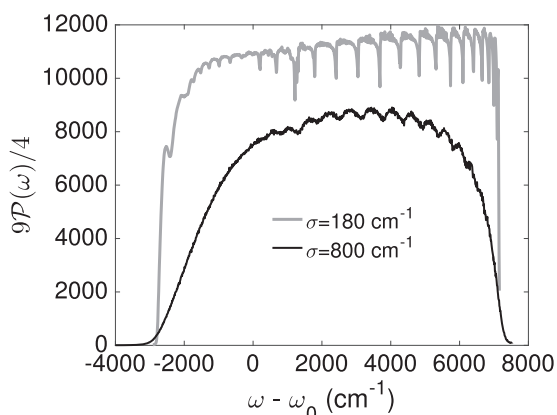
FIG. 5. The participation number over the whole exciton band for tubes with $N_2 = 11$ and $N_1 = 666$ for two values of the disorder. The scaling factor 9/4 was introduced to recover the system size in case $\sigma = 0$ (see text).

growing disorder, for each energy, the states become more localized; furthermore, the localization is stronger near the band edges than at the band center, as is common for disordered systems.[32,71] Inside the exciton band, most clearly for $\sigma = 180$ cm^{-1}, the participation number exhibits a structure with dips occurring at discrete energy positions. This is similar to the dip found in one-dimensional disordered systems[32] and reflects the persistence of the quasi-one dimensional exciton sub-bands characterized by the quantum number k_2 for weak disorder. For $\sigma = 180$ cm^{-1}, the value of the participation number (scaled by the factor 9/4) inside the exciton band indeed reflects the participation of almost all 14 652 molecules in the exciton wave functions, i.e., practically complete delocalization.

Next, we investigate the dependence of the participation number on the tube's size (length and radius). We are mainly interested in the eigenstates in the optically relevant region of the low-energy absorption band, where localization effects are strong. To this end, we calculate the average participation number of the exciton states in the region of ± 80 cm^{-1} around the peak position of the lowest-energy J band of the homogeneous aggregate, $\approx 16\,280$ cm^{-1} (the exact numbers for each system are given in the Appendix, Tables I and II) denoted as $\mathcal{P}(\omega_J)$.

Figure 6 (top panels) shows $9\mathcal{P}(\omega_J)/4$ as a function of the tube's length and radius for the homogeneous system (green) and for two values of the disorder: $\sigma = 180$ cm^{-1} (blue) and $\sigma = 800$ cm^{-1} (red). For the length dependence, the radius of the tubes is fixed at $N_2 = 6$, and the length increases from $N_1 = 666$ to $N_1 = 2500$. In the case of the radius dependence, the length is fixed at $N_1 = 666$, and the radius increases from $N_2 = 1$ to $N_2 = 35$. In the homogeneous limit, the participation number (corrected by the factor 9/4) correctly is seen to grow linearly with the system size and to be basically equal to this size (in this case $12N_1$), reflecting complete delocalization. Disorder suppresses the exciton delocalization and, therefore, decreases the participation number. For $\sigma = 180$ cm^{-1}, the participation number still increases with the system size over the entire region of the length and radius considered, meaning that the delocalization size, even for the largest sizes considered, still is limited by the system size and not by the disorder. This clearly reflects the weak character of the exciton localization due to the higher-dimensional character

of the tubes. The radius dependence persists longer than the length dependence, which for $N_2 = 6$ starts to saturate around a length of 1500 rings. This is also seen for the stronger value of the disorder, $\sigma = 800$ cm^{-1}, where the length dependence is quite weak for $N_2 = 6$, implying that the delocalization of the exciton states along the tube's axis is not limited by its length for this disorder strength, while the delocalization size grows for growing radius over the entire N_2 domain studied.

The strong radius dependence of the delocalization sizes prompted us to introduce the reduced participation number, defined by the participation number divided by the number of molecules per ring, $\mathcal{P}_{\text{red}} = \mathcal{P}/(2N_2)$. For states that are completely delocalized around the circumference of the tube, $\mathcal{P}_{\text{red}}$ is expected to be constant as a function of N_2. This number may then be interpreted as the number of rings along the tube over which the exciton states are delocalized. The reduced participation number as a function of length and radius is shown in the bottom panels of Fig. 6, again for $\sigma = 180$ cm^{-1} and 800 cm^{-1}. We first discuss the data for $\sigma = 180$ cm^{-1}. It is clearly seen that for small N_2 values, up to about $N_2 = 6$, $\mathcal{P}_{\text{red}}$ is not a constant but grows strongly with N_2. This means that not only the states are fully delocalized around the rings but also that, moreover, the number of rings over which the states are delocalized grows with an increase in radius. This supralinear dependence of the total participation number on the radius finds its origin in intra-ring exchange narrowing of the disorder: states that are completely delocalized around each ring have k_2 states whose energy distribution imposed by the disorder does not have a width given by σ but rather by $\sigma/\sqrt{2N_2}$. In a perturbative picture, for each k_2 value, this leads to an effective one-dimensional chain (of rings) with the effective energy disorder strength $\sigma^* = \sigma/\sqrt{2N_2}$, i.e., an effective disorder strength that diminishes with growing radius. This explains that the exciton delocalization along the tube's axis can grow with an increase in radius. Using the disorder scaling of the delocalization size in linear chains found in Ref. 32, the number of rings that participate in the wave functions is expected to scale as $\sigma^{*(-2/3)} \sim N_2^{1/3}$. The actual scaling deduced from the first four data points for $\mathcal{P}_{\text{red}}$ for $\sigma = 180$ cm^{-1} is best fit to a scaling relation $\sim N_2^{1/2}$. Given the difficulty in deducing a good power-law fit from just four data points and the fact that the perturbative arguments used here are bound to break down quite easily for the high density of states in the system considered, the differences of the two exponents is not unreasonable. Beyond $N_2 \approx 6$, $\mathcal{P}_{\text{red}}$ for $\sigma = 180$ cm^{-1} starts to saturate toward a constant: the number of rings that participate in the exciton wave functions hardly grows anymore. Closer inspection shows that this saturation is governed by the tube's length, i.e., the delocalization size for $N_2 > 6$ is strongly limited by the tube's length. This is made explicit by the additional data point in the lower-right panel of Fig. 6, which indicates $\mathcal{P}_{\text{red}}$ for $N_2 = 6$ and $N_1 = 2500$.

For the stronger disorder value considered ($\sigma = 800$ cm^{-1}), intra-ring exchange narrowing also seems to occur for small radii but much less pronounced than for the case of weak disorder (see the inset in the lower-right panel of Fig. 6 for details). Moreover, following the saturation around $N_2 = 8$, $\mathcal{P}_{\text{red}}$ starts to diminish with growing radius, implying that the states are no longer fully delocalized around the tube's circumference. The delocalization for this disorder strength is not limited by the chain length of $N_1 = 666$ rings, not even for the largest radii.
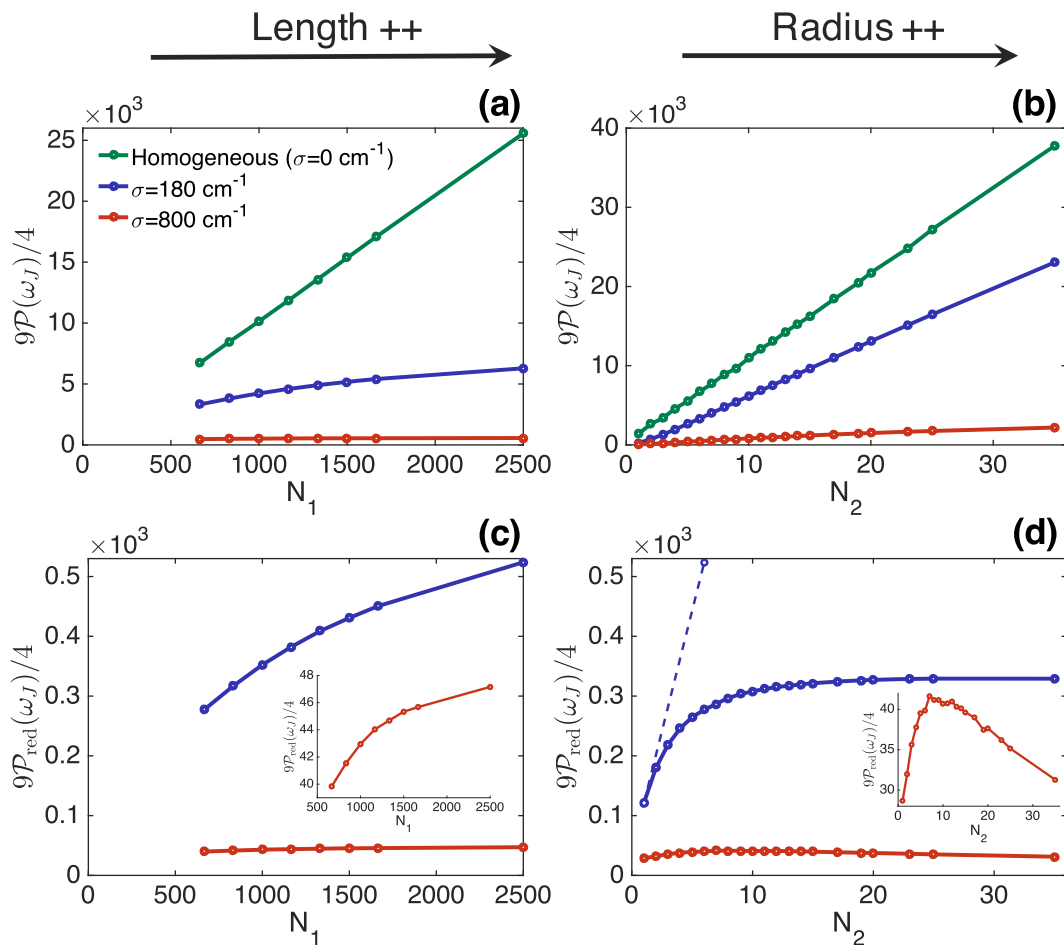
FIG. 6. Length and radius dependence of the degree of exciton localization. [(a) and (b)] The participation number and [(c) and (d)] the reduced participation number near the peak position of the lowest-energy J band are shown as a function of system size for two values of the disorder strength: $\sigma = 180$ cm^{-1} and $\sigma = 800$ cm^{-1}. The length dependence (left panels) is shown for tubes with a fixed radius ($N_2 = 6$) and the length varying from $N_1 = 666$ to $N_1 = 2500$. The radius dependence (right panels) is presented for tubes with a fixed length ($N_1 = 666$) and the radius varying from $N_2 = 1$ to $N_2 = 35$. The insets in the bottom panels show blow-ups of the dependence for $\sigma = 800$ cm^{-1}. The additional data point in the bottom-right panel for $\sigma = 180$ cm^{-1} (connected by the dashed line) indicates the value for $N_2 = 6$ for a longer tube ($N_1 = 2500$).

C. Extent of the wave function from its autocorrelation function

As mentioned in Sec. II, an alternative measure of the degree of delocalization is the auto-correlation function of the exciton wave function, which has the advantage that for higher-dimensional systems, it also gives directional information. In this section, we use the auto-correlation function defined in Eq. (6), and we will be particularly interested in its dependence along the direction of the tube's axis, i.e., in $C(s_1, s_2 = 0; \omega)$ as a function of the relative separation s_1 between two rings. As before, we will be particularly interested in the energy region ω_J around the lowest-energy J band.

Figure 7 shows the typical autocorrelation function for a homogeneous tube with $N_1 = 1166$ and $N_2 = 6$ [Fig. 7(a)] and the same tube in the presence of strong disorder $\sigma = 800$ cm^{-1} [Fig. 7(b)]. As can be seen from the 3D correlation plot, the exciton wave function

of the homogeneous system [Fig. 7(a)] is extended over the whole aggregate with a steep drop of the correlation function at the edges of the tube due to the open boundary conditions. In the s_2 direction, such a drop does not occur because of the circular nature of this coordinate. For the disordered system [Fig. 7(b)], the autocorrelation function at $\omega = \omega_J$ shows a peak with a maximum value 1 at the origin, $(s_1, s_2) - (0, 0)$, and a drop in both s_1 (longitudinal) and s_2 (circumferential) directions. It can be seen, though, that a high correlation along s_2 is preserved, which supports the idea that the states at ω_J still are quite strongly delocalized along the rings for this circumference, even for $\sigma = 800$ cm^{-1}. As we are particularly interested in the direction of the tube's axis, we study the decay of the correlation function $C(s_1, s_2 = 0; \omega)$, highlighted by the red line in Fig. 7(b). Initially, the correlation function follows a power-law decay, which only is important for a few rings close to the origin, while at larger distances, the decay is exponential. This is in
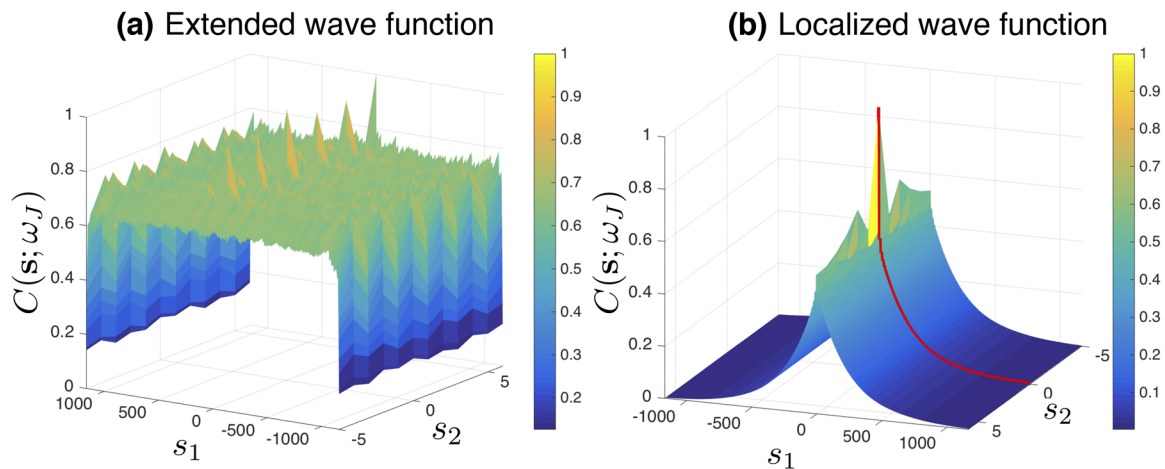
FIG. 7. Typical autocorrelation function of the exciton wave function. Plotted is $C(\mathbf{s}; \omega_J)$ for a (a) homogeneous ($\sigma = 0$ cm^{-1}) and (b) disordered tube ($\sigma = 800$ cm^{-1}) with $N_1 = 1166$ and $N_2 = 6$. The correlation function $C(s_1, s_2 = 0; \omega)$ is highlighted by the red line.

agreement with a previous numerical study of 1D, 2D, and 3D disordered electronic systems,[72] where it was concluded that a power-law decay of the wave functions mediates between extended states and strongly localized states with exponential decay.

Figure 8 shows the correlation length in the longitudinal direction $N_{\parallel,\text{corr}}$ [defined above in Eq. (6)] as a function of the tube's length and radius. In Fig. 8(a), it is seen that for weak disorder ($\sigma = 180$ cm^{-1}), $N_{\parallel,\text{corr}}$ grows with the tube's length up to a length of about $N_1 = 1000$, after which it reaches a plateau with $N_{\parallel,\text{corr}} \approx 870$. This means that for tubes with $N_2 = 6$ and shorter than about 1000 rings, the physical size is the limiting factor for the correlation length. This matches the saturation of the increase in the participation number seen in Fig. 6(a) around $N_1 = 1000$–1500. As shown

in Fig. 7(a), for $\sigma = 800$ cm^{-1}, the disorder is the limiting factor for $N_{\parallel,\text{corr}}$, which again matches the behavior seen in Fig. 6(a).

As is seen in Fig. 8(b), for weak disorder, $N_{\parallel,\text{corr}}$ grows linearly with the radius for small values of N_2, while a plateau is observed for values of $N_2 > 5$. This plateau results from a physical limitation, namely, the length $N_1 = 666$ of the tubes considered, in case we study the radius dependence. This is confirmed by also calculating the correlation length for $N_1 = 1000$ and $N_2 = 6$ [additional data point in Fig. 8(b) connected by a dashed line]. The linear dependence of the correlation length on N_2 appears to persist until $N_2 = 6$. This behavior is in agreement with the fact that the reduced participation ratio in Fig. 6(d) initially grows with the radius, albeit that there the increase was not found to be linear. Again, the increase in
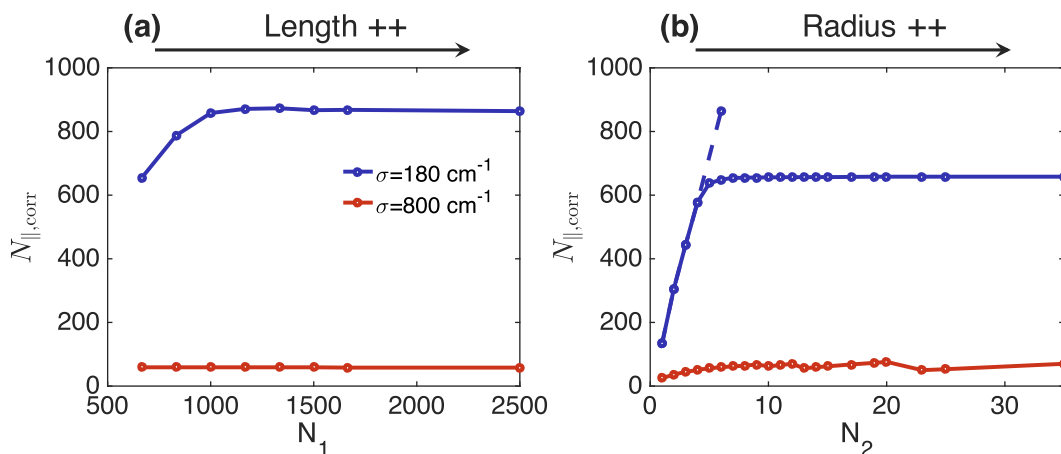
FIG. 8. Correlation length as a function of the tube's length and radius. (a) The length dependence is calculated for tubes with a fixed radius ($N_2 = 6$) and a length varying from $N_1 = 666$ to $N_1 = 2500$. (b) The radius dependence is determined for tubes with a fixed length ($N_1 = 666$) and a radius varying from $N_2 = 1$ to $N_2 = 35$. The additional data point connected to the others by a dashed line is obtained for $N_1 = 1000$ and $N_2 = 6$.
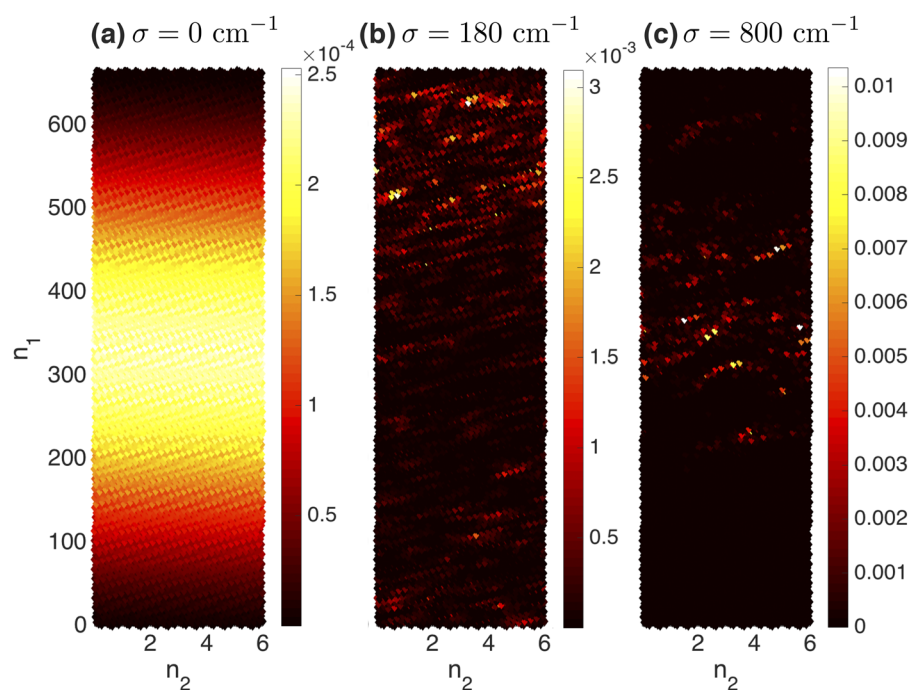
FIG. 9. The probability density for wave functions in the low-energy region is plotted on the unwrapped surface for tubes with $N_2 = 6$ and $N_1 = 666$: (a) in the absence of disorder, (b) for $\sigma = 180$ cm^{-1}, and (c) for $\sigma = 800$ cm^{-1}.

the correlation length with the increase in the tube's radius results from the intra-ring exchange narrowing effect. For $\sigma = 800$ cm^{-1}, the radius dependence of the correlation length closely matches that of the reduced participation number found in Fig. 6(d).

D. Character of the exciton wave function

The participation number and autocorrelation function give statistical information on the characteristics of the exciton wave functions. It is also interesting, though, to consider examples of typical wave functions for a specific realization of the disorder. To this end, we show in Fig. 9 the probability density $|\varphi_{kn}|^2$ on the unwrapped surface of the cylinder for typical exciton states near the lowest-energy J band for tubes with $N_1 = 666$ and $N_2 = 6$ with $\sigma = 0$ cm^{-1}, 180 cm^{-1}, and 800 cm^{-1}. For a homogeneous tube [Fig. 9(a)], the $k_2 = 0$ exciton state has equal amplitude on all unit cells within the same ring, while along the tube's axis, the probability density resembles the lowest exciton state in a linear J-aggregate, having a maximum at the center of the tube's axis and decaying toward the edges. The alternating pattern, observed most clearly in the homogeneous case, is due to the presence of two molecules in each unit cell. The chirality observed follows the direction of the strongest interaction between neighboring rings. For weak disorder [Fig. 9(b)], the probability density is extended over the whole tube, however, in a quite scattered way, similar to the fractal character of quasi-particle states reported in disordered two-dimensional systems.[61,73] For stronger disorder [Fig. 9(c)], the probability density of the wave function is more concentrated (localized) on a specific part of the cylinder (here the center). The specific, fractal-like nature of the exciton wave functions at weak disorder strengths may be responsible for the large values of both the correlation lengths and

the reduced participation numbers found for $\sigma = 180$ cm^{-1} described in Secs. III B and III C.

IV. CONCLUSIONS

In this paper, we systematically examined the dependence of the exciton localization and optical properties on both the radius and the length of tubular molecular aggregates. As a specific model, we used the structure previously reported to model the inner wall of C8S3 aggregates, described by an extended herringbone model with two molecules per unit cell. We numerically calculated the absorption spectra in the presence of Gaussian diagonal disorder for tubes of various lengths (up to 740 nm) and radii (up to 20.7 nm). We found that the effect of the tube's length, observed as a red-shift of the lowest-energy band with an increase in length, is still visible for tubes as long as 150 nm. The effect of the radius is much more pronounced due to the strong dependence of the higher-energy bands polarized perpendicular to the tube's axis on its radius.

We used two quantities to study the localization behavior as a function of the length and radius: the (reduced) participation number that gives a measure for the typical number of molecules participating in the exciton states at a particular energy and the autocorrelation function of the exciton wave function that gives statistical information on the extent and the directionality of the exciton wave functions. The obtained results suggest that the physical size rather than the disorder is the limiting factor for the delocalization of the exciton states of C8S3 cyanine aggregates, at least for aggregates shorter than about 1 μm. It should be noted that the length dependence of the localization size does not seem to affect the absorption

spectrum, except for lengths smaller than 150 nm. In general, we found that for the disorder value relevant to C8S3 aggregates ($\sigma = 180$ cm^{-1}), the exciton wave functions in the optically important region of the lowest-energy J band are fully delocalized around the circumference of the tubes, which is consistent with the strong polarization properties found in the experimental absorption spectrum of these aggregates.[38] Moreover, this circumferential delocalization persists up to large radii, even larger than those considered in our calculations. This, *inter alia*, gives rise to the interesting effect of intra-ring exchange narrowing of disorder, which ultimately results in the growth of the delocalization length along the axis direction of the aggregate with growing radius. The excitonic states in the middle of the exciton band are hardly affected by static disorder, even for strong disorder values of more than 1000 cm^{-1}. Conversely, states at the lower edge of the exciton band (close to the lowest-energy J band), as well as the upper edge, show stronger localization effects than those in the optically dominant region, but they still are very delocalized.

The properties of the exciton states found here are of interest in their own right, in the realm of localization problems, and for the optical absorption of the system, namely, to identify the character of the states that are responsible for the absorption process. They may also have a bearing on dynamic processes, such as exciton transport, which was shown to occur with a higher diffusion constant for larger delocalization lengths.[59] In that case, however, a more in-depth study is also needed to assess the importance of dynamic disorder, giving rise to dephasing, which over time may destroy coherences between different molecules, in particular, distant ones. In addition, we note that in this work, we have restricted ourselves to the long-wavelength approximation and near-field $1/r^3$ dipolar interactions. For the longest aggregates considered here, the inclusion of radiative corrections in the interactions[30,31,74] and accounting for the spatial dependence of the applied electric field[75] potentially lead to new effects, which would be interesting to explore further in a future study.

DATA AVAILABILITY

The data that support the findings of this study are available from the corresponding author upon reasonable request.

APPENDIX: ADDITIONAL INFORMATION ABOUT MODELED STRUCTURES

1. Length distribution

For the length dependence studies, the radius of the tubes was kept fixed, while the length was varied from 50 nm up to 740 nm (see Table I). The radius was chosen to be equal to 3.5505 nm, which corresponds to $N_2 = 6$ unit cells in the ring, as is the case for the inner wall of C8S3 aggregates.[39]

TABLE I. Model tubes used for length dependence study. N_1 is the number of the rings in the tube, L is the length of the tube, N is the total number of molecules, ω ($k_2 = 0$) is the frequency of the low-energy Davydov component of the $k_2 = 0$ band, and the bandwidth refers to the width of the exciton band of the tube without disorder.

N_1	L (nm)	N	Bandwidth (cm^{-1})	ω ($k_2 = 0$) (cm^{-1})
170	50.3	2 040	16 113.2–25 991.8	16 339
340	100.5	4 080	16 111.8–25 995.0	16 299
510	150.8	6 120	16 111.5–25 995.6	16 288
666	196.9	7 992	16 111.4–25 995.8	16 283
833	246.2	9 996	16 111.4–25 995.9	16 281
1000	295.6	12 000	16 111.3–25 995.9	16 279
1166	344.7	13 992	16 111.3–25 996.0	16 278
1333	394.0	15 996	16 111.3–25 996.0	16 277
1500	443.4	18 000	16 111.3–25 996.0	16 277
1666	492.5	19 992	16 111.3–25 996.0	16 276
2500	739.0	30 000	16 111.3–25 996.0	16 275

2. Radius distribution

For the modeling of the radius dependence, the same lattice of the inner wall of C8S3 was used, where the radius was defined by the number of unit cells on the rolling vector (in order to preserve the rolling angle, only specific radii can be taken, namely, when the end point of the rolling vector coincides with a lattice point). The radii considered are given in Table II. The length of the tubes was then kept fixed at 196.9 nm.

TABLE II. Model tubes used for the radius dependence study. N_2 is the number of unit cells in the ring, R is the radius, and N is the total number of molecules. The bandwidth and ω ($k_2 = 0$) are as defined in the caption of Table I.

N_2	R (nm)	N	Bandwidth (cm^{-1})	ω ($k_2 = 0$) (cm^{-1})
1	0.5918	1 332	15 950.2–24 885.7	16 355
2	1.1835	2 664	16 080.7–25 900.1	16 273
3	1.7753	3 996	16 103.4–25 878.2	16 276
4	2.3670	5 328	16 109.1–25 980.4	16 279
5	2.9588	6 660	16 110.6–25 961.4	16 281
6	3.5505	7 992	16 111.4–25 995.8	16 283
7	4.1423	9 324	16 112.0–25 984.3	16 284
8	4.7340	10 656	16 112.4–26 001.2	16 286
9	5.3258	11 988	16 112.8–25 993.8	16 287
10	5.9175	13 320	16 113.0–26 003.7	16 287
11	6.5093	14 652	16 113.3–25 998.6	16 288
12	7.1011	15 984	16 113.4–26 005.1	16 289
13	7.6928	17 316	16 113.6–26 001.3	16 290
14	8.2846	18 648	16 113.7–26 005.9	16 290
15	8.8763	19 980	16 113.8–26 003.0	16 291
17	10.06	22 644	16 114.0–26 004.2	16 292
19	11.243	25 308	16 114.1–26 005.0	16 293
20	11.835	26 640	16 114.2–26 007.1	16 293
23	13.61	30 636	16 114.3–26 006.0	16 294
25	14.794	33 300	16 114.3–26 006.4	16 295
35	20.711	46 620	16 114.4–26 007.3	16 297

As mentioned in the main text, the radius of the tube with $N_2 = 6$ corresponds to the inner wall of the C8S3 aggregate, while the one with $N_2 = 11$ agrees with the inner wall of the bromine-substituted C8S3 aggregate (without adjusting the other structural parameters).[39,60]

REFERENCES

[1] E. E. Jelley, Nature **138**, 1009 (1936).

[2] E. E. Jelley, Nature **139**, 631 (1937).

[3] G. Scheibe, Angew. Chem. **50**, 212 (1937).

[4] E. W. Knapp, Chem. Phys. **85**, 73 (1984).

[5] V. A. Malyshev and F. Domínguez-Adame, Chem. Phys. Lett. **313**, 255 (1999).

[6] S. De Boer and D. A. Wiersma, Chem. Phys. Lett. **165**, 45 (1990).

[7] H. Fidder, J. Knoester, and D. A. Wiersma, Chem. Phys. Lett. **171**, 529 (1990).

[8] H. Fidder, J. Knoester, and D. A. Wiersma, J. Chem. Phys. **98**, 6564 (1993).

[9] G. Juzeliunas, Z. Phys, D At., Mol. Clusters **8**, 379 (1988).

[10] F. C. Spano and S. Mukamel, Phys. Rev. A **40**, 5783 (1989).

[11] J. Knoester, Chem. Phys. Lett. **203**, 371 (1993).

[12] I. G. Scheblykin, O. Y. Sliusarenko, L. S. Lepnev, A. G. Vitukhnovsky, and M. Van der Auweraer, J. Phys. Chem. B **105**, 4636 (2001).

[13] T. Tani, *Photographic Sensitivity: Theory and Mechanisms* (Oxford University Press on Demand, 1995), Vol. 8.

[14] A. H. Herz, Adv. Colloid Interface Sci. **8**, 237 (1977).

[15] C. E. K. Mees, *The Theory of the Photographic Process* (Macmillan Co., New York, 1942).

[16] G. D. Scholes, G. R. Fleming, A. Olaya-Castro, and R. van Grondelle, Nat. Chem. **3**, 763 (2011).

[17] G. S. Orf and R. E. Blankenship, Photosynth. Res. **116**, 315 (2013).

[18] M. Schulze, V. Kunz, P. D. Frischmann, and F. Würthner, Nat. Chem. **8**, 576 (2016).

[19] S. J. Jang and B. Mennucci, Rev. Mod. Phys. **90**, 035003 (2018).

[20] A. M. van Oijen, M. Ketelaars, J. Köhler, T. J. Aartsma, and J. Schmidt, Science **285**, 400 (1999).

[21] S. Jang, S. E. Dempster, and R. J. Silbey, J. Phys. Chem. B **105**, 6655 (2001).

[22] P. Reineker, C. Warns, C. Supritz, and I. Barvík, J. Lumin. **102**, 802 (2003).

[23] G. S. Engel, T. R. Calhoun, E. L. Read, T.-K. Ahn, T. Mančal, Y.-C. Cheng, R. E. Blankenship, and G. R. Fleming, Nature **446**, 782 (2007).

[24] J. Wu, F. Liu, J. Ma, R. J. Silbey, and J. Cao, J. Chem. Phys. **137**, 174111 (2012).

[25] L. Cleary and J. Cao, New J. Phys. **15**, 125030 (2013).

[26] R. Tempelaar, T. L. C. Jansen, and J. Knoester, J. Phys. Chem. B **118**, 12865 (2014).

[27] G. D. Scholes, G. R. Fleming, L. X. Chen, A. Aspuru-Guzik, A. Buchleitner, D. F. Coker, G. S. Engel, R. Van Grondelle, A. Ishizaki, D. M. Jonas *et al.*, Nature **543**, 647 (2017).

[28] H.-G. Duan, V. I. Prokhorenko, R. J. Cogdell, K. Ashraf, A. L. Stevens, M. Thorwart, and R. J. D. Miller, Proc. Natl. Acad. Sci. **114**, 8493 (2017).

[29] E. Thyrhaug, R. Tempelaar, M. J. P. Alcocer, K. Žídek, D. Bína, J. Knoester, T. L. C. Jansen, and D. Zigmantas, Nat. Chem. **10**, 780 (2018).

[30] M. Gullì, A. Valzelli, F. Mattiotti, M. Angeli, F. Borgonovi, and G. L. Celardo, New J. Phys. **21**, 013019 (2019).

[31] G. L. Celardo, M. Angeli, T. J. A. Craddock, and P. Kurian, New J. Phys. **21**, 023005 (2019).

[32] H. Fidder, J. Knoester, and D. A. Wiersma, J. Chem. Phys. **95**, 7880 (1991).

[33] C. Spitz, J. Knoester, A. Ouart, and S. Daehne, Chem. Phys. **275**, 271 (2002).

[34] C. Spitz and S. Daehne, Int. J. Photoenergy **2006**, 84950 (2006).

[35] S. C. M. Gandini, E. L. Gelamo, R. Itri, and M. Tabak, Biophys. J. **85**, 1259 (2003).

[36] S. M. Vlaming, R. Augulis, M. C. A. Stuart, J. Knoester, and P. H. M. Van Loosdrecht, J. Phys. Chem. B **113**, 2273 (2009).

[37] A. Pawlik, S. Kirstein, U. De Rossi, and S. Daehne, J. Phys. Chem. B **101**, 5646 (1997).

[38] C. Didraga, A. Pugžlys, P. R. Hania, H. von Berlepsch, K. Duppen, and J. Knoester, J. Phys. Chem. B **108**, 14976 (2004).

[39] D. M. Eisele, C. W. Cone, E. A. Bloemsma, S. M. Vlaming, C. G. F. van der Kwaak, R. J. Silbey, M. G. Bawendi, J. Knoester, J. P. Rabe, and D. A. Vanden Bout, Nat. Chem. **4**, 655 (2012).

[40] K. A. Clark, C. W. Cone, and D. A. Vanden Bout, J. Phys. Chem. C **117**, 26473 (2013).

[41] J. Sperling, A. Nemeth, J. Hauer, D. Abramavicius, S. Mukamel, H. F. Kauffmann, and F. Milota, J. Phys. Chem. A **114**, 8179 (2010).

[42] D. Abramavicius, A. Nemeth, F. Milota, J. Sperling, S. Mukamel, and H. F. Kauffmann, Phys. Rev. Lett. **108**, 067401 (2012).

[43] J. Yuen-Zhou, D. H. Arias, D. M. Eisele, C. P. Steiner, J. J. Krich, M. G. Bawendi, K. A. Nelson, and A. Aspuru-Guzik, ACS Nano **8**, 5527 (2014).

[44] E. Lang, A. Sorokin, M. Drechsler, Y. V. Malyukin, and J. Köhler, Nano Lett. **5**, 2635 (2005).

[45] S. Sengupta, D. Ebeling, S. Patwardhan, X. Zhang, H. von Berlepsch, C. Böttcher, V. Stepanenko, S. Uemura, C. Hentschel, H. Fuchs, F. C. Grozema, L. D. A. Siebbeles, A. R. Holzwarth, L. Chi, and F. Würthner, Angew. Chem., Int. Ed. **51**, 6378 (2012).

[46] H. v. Berlepsch and C. Böttcher, Langmuir **29**, 4948 (2013).

[47] A. V. Sorokin, I. I. Filimonova, R. S. Grynyov, G. Y. Guralchuk, S. L. Yefimova, and Y. V. Malyukin, J. Phys. Chem. C **114**, 1299 (2010).

[48] J. M. Womick, S. A. Miller, and A. M. Moran, J. Phys. Chem. A **113**, 6587 (2009).

[49] J. M. Womick, S. A. Miller, and A. M. Moran, J. Phys. Chem. B **113**, 6630 (2009).

[50] S. Doria, T. S. Sinclair, N. D. Klein, D. I. G. Bennett, C. Chuang, F. S. Freyria, C. P. Steiner, P. Foggi, K. A. Nelson, J. Cao, A. Aspuru-Guzik, S. Lloyd, J. R. Caram, and M. G. Bawendi, ACS Nano **12**, 4556 (2018).

[51] J. R. Caram, S. Doria, D. M. Eisele, F. S. Freyria, T. S. Sinclair, P. Rebentrost, S. Lloyd, and M. G. Bawendi, Nano Lett. **16**, 6808 (2016).

[52] B. Kriete, J. Lüttig, T. Kunsel, P. Malý, T. L. C. Jansen, J. Knoester, T. Brixner, and M. S. Pshenichnikov, Nat. Commun. **10**, 4615 (2019).

[53] A. Löhner, T. Kunsel, M. I. S. Röhr, T. L. C. Jansen, S. Sengupta, F. Würthner, J. Knoester, and J. Köhler, J. Phys. Chem. Lett. **10**, 2715 (2019).

[54] A. R. Holzwarth and K. Schaffner, Photosynth. Res. **41**, 225 (1994).

[55] S. Ganapathy, G. T. Oostergetel, P. K. Wawrzyniak, M. Reus, A. G. M. Chew, F. Buda, E. J. Boekema, D. A. Bryant, A. R. Holzwarth, and H. J. M. de Groot, Proc. Natl. Acad. Sci. U. S. A. **106**, 8525 (2009).

[56] Y. Tian, R. Camacho, D. Thomsson, M. Reus, A. R. Holzwarth, and I. G. Scheblykin, J. Am. Chem. Soc. **133**, 17192 (2011).

[57] L. M. Günther, M. Jendrny, E. A. Bloemsma, M. Tank, G. T. Oostergetel, D. A. Bryant, J. Knoester, and J. Köhler, J. Phys. Chem. B **120**, 5367 (2016).

[58] E. A. Bloemsma, S. M. Vlaming, V. A. Malyshev, and J. Knoester, Phys. Rev. Lett. **114**, 156804 (2015).

[59] C. Chuang, C. K. Lee, J. M. Moix, J. Knoester, and J. Cao, Phys. Rev. Lett. **116**, 196803 (2016).

[60] B. Kriete, A. S. Bondarenko, V. R. Jumde, L. E. Franken, A. J. Minnaard, T. L. C. Jansen, J. Knoester, and M. S. Pshenichnikov, J. Phys. Chem. Lett. **8**, 2895 (2017).

[61] M. Schreiber and H. Grussbach, Phys. Rev. Lett. **67**, 607 (1991).

[62] D. J. Thouless, Phys. Rep. **13**, 93 (1974).

[63] M. Schreiber and Y. Toyozawa, J. Phys. Soc. Jpn. **51**, 1537 (1982).

[64] C. Didraga and J. Knoester, J. Chem. Phys. **121**, 10687 (2004).

[65] C. Didraga, J. A. Klugkist, and J. Knoester, J. Phys. Chem. B **106**, 11474 (2002).

[66] B. Kriete and M. S. Pshenichnikov, private communication (2020).

[67] M. Schreiber and Y. Toyozawa, J. Phys. Soc. Jpn. **51**, 1528 (1982).

[68] A. Boukahil and D. L. Huber, J. Lumin. **45**, 13 (1990).

[69] J. Köhler, A. Jayannavar, and P. Reineker, Z. Phys. B: Condens. Matter **75**, 451 (1989).

[70] V. Malyshev and P. Moreno, Phys. Rev. B **51**, 14587 (1995).

[71] P. W. Anderson, Phys. Rev. **109**, 1492 (1958).

[72] M. Schreiber, J. Phys. C: Solid State Phys. **18**, 2493 (1985).

[73] H. Aoki, J. Phys. C: Solid State Phys. **16**, L205 (1983).

[74] F. C. Spano and S. Mukamel, J. Chem. Phys. **91**, 683 (1989).

[75] F. C. Spano, J. Chem. Phys. **96**, 8109 (1992).